

Bethe-Salpeter wave functions of $\eta_c(2S)$ and $\psi(2S)$ states from full lattice QCD

Kazuki Nochi^{1,*}, Taichi Kawanai^{2,†} and Shoichi Sasaki^{1,‡}

¹*Department of Physics, Tohoku University, Sendai 980-8578, Japan and*

²*Jülich Supercomputing Center, Jülich D-52425, Germany*

(Dated: September 22, 2021)

We discuss the internal structure of radially excited charmonium mesons based on the equal-time and Coulomb gauge Bethe-Salpeter (BS) amplitudes, which are obtained in lattice QCD. Our simulations are performed with a relativistic heavy-quark action for the charm quark on the (2+1)-flavor PACS-CS gauge configurations at the lightest pion mass, $M_\pi = 156(7)$ MeV. The variational method is applied to the study of the optimal charmonium operators for ground and first excited states of S -wave charmonia. We successfully calculate the BS wave functions of $\eta_c(2S)$ and $\psi(2S)$ states, as well as $\eta_c(1S)$ and J/ψ states, and then estimate the root-mean-square radii of both the $1S$ and $2S$ charmonium states. We also examine whether a series of the BS wave functions from the ground state to excited states can be described by a single set of the spin-independent and spin-dependent interquark potentials with a unique quark mass. It is found that the quark kinetic mass and both the central and the spin-spin charmonium potentials, determined from the $2S$ wave functions, fairly agree with the ones from the $1S$ wave functions. This strongly supports the validity of the potential description for the charmonium system—at least, below the open-charm threshold.

I. INTRODUCTION

The constituent quark description of the heavy quarkonium systems has been successful in aiding the qualitative understanding of properties of the charmonium and bottomonium states, especially below the thresholds for decays to mesons with open heavy flavor [1–3]. The complicated dynamics of quarks and gluons in QCD could be described by the *interquark potential* within the framework of nonrelativistic quantum mechanics due to the heavy degrees of freedom whose energy scale is much higher than the QCD scale (Λ_{QCD}). Such nonrelativistic potential (NRp) models share a common feature on the interquark potential that incorporates two types of underlying physics: the Coulombic potential, which dominates in short range in accordance with the asymptotic freedom of QCD, and a long-range potential responsible for the quark confinement [1–3].

For the heavy quarkonium systems, the Cornell potential is often adopted, and its functional form is given by

$$V(r) = -\frac{A}{r} + \sigma r + V_0, \quad (1)$$

where A is the Coulombic coefficient, σ denotes the string tension, and V_0 is the constant term associated with a self-energy contribution of the color sources [1]. If one-gluon exchange is responsible for the Coulombic term, the coefficient A is associated with the strong coupling constant α_s as $A = \frac{4}{3}\alpha_s$.

Although the Cornell potential was not directly derived from QCD, the functional form has been qualitatively justified by the static heavy quark potential obtained from Wilson loops in lattice QCD [4]. There are

slight differences in terms of the Cornell parameters (A , σ) between the phenomenological potential used in the NRp models and the Wilson-loop results. This is simply because the resulting *static potential* from Wilson loops is defined in the infinitely heavy quark limit [4].

The finite-mass correction should be somewhat taken into account for the Wilson-loop results. Such corrections to the static potential are classified in powers of the inverse of both heavy quark mass m_Q and quark momentum $m_Q v$ (relative quark velocity v) within the modern approach of effective field theory called potential nonrelativistic QCD (pNRQCD) [5]. In line with the framework of pNRQCD, the $\mathcal{O}(1/m_Q)$ correction [6] and the $\mathcal{O}(1/m_Q^2)$ spin-dependent corrections [7] to the static potential have been computed in *quenched* QCD.

The charm quark mass region is far outside the validity region for the $1/m_Q$ expansion [4]. Moreover, the convergence behavior seems to be questionable even at the bottom mass region. Indeed, a spin-spin potential determined at $\mathcal{O}(1/m_Q^2)$ from lattice QCD exhibits a slightly “attractive” interaction for the case of spin-triplet states [7]. It implies that a breakdown of the adiabatic approximation is not avoided even at the bottom sector, since the leading-order contribution of the spin-spin potential yields *wrong mass ordering among hyperfine multiplets* [8].

An interesting idea to define a two-body potential from the equal-time Bethe-Salpeter (BS) amplitude was proposed by Aoki, Hatsuda, and Ishii for studying the nuclear force in lattice QCD [9, 10]. Subsequently, Ikeda and Iida applied the same idea to the quarkonium system in order to compute the interquark potential without the adiabatic approximation [11, 12]. These preceding studies led us to propose a novel approach, where both the quark kinetic mass and the interquark potential are self-consistently determined within the BS amplitude method, in order to obtain *proper interquark potential at finite quark mass* using lattice QCD [13].

*Electronic address: nochi@nucl.phys.tohoku.ac.jp

†Electronic address: t.kawanai@fz-juelich.de

‡Electronic address: ssasaki@nucl.phys.tohoku.ac.jp

We have elaborated the new approach to determine reliable interquark potential from lattice QCD in our previous works [13–16]. In this work, we will discuss the internal structure of the radially excited charmonium mesons as a further application of the BS amplitude method.

It is frequently asked whether a universal interquark potential and a unique quark mass can be simultaneously defined in a series of the BS amplitudes from the ground state to excited states. This question is aimed at the validity of the potential description for the heavy quarkonium systems and also the reliability of the interquark potential determined from the BS amplitudes. In an attempt to settle these points, we will verify the validity of the BS amplitude method through a direct comparison of the charmonium potentials which are independently evaluated from the BS wave functions of either the ground or first radially excited charmonium mesons in lattice QCD simulations.

This paper is organized as follows: In Sec. II, we describe an implementation of the variational method [17, 18] in the calculation of the BS wave functions for both the ground and radially excited states. Subsequently, we give a brief review of two methods for determination of the interquark potential including the quark kinetic mass from the resulting BS wave functions. Section III gives the numerical details in calculating the BS wave functions of both the ground (1S) and first radially excited (2S) states for the S-wave charmonia. In Sec. III, we also discuss the validity of the potential description for the charmonium system through a direct comparison between the interquark potentials that are independently determined by both the 1S and 2S charmonium states. Finally, we close with a brief summary and our conclusions in Sec. IV.

II. FORMALISM

A. BS wave functions determined through the variational method

The equal-time BS amplitude for the n th meson is defined by

$$\phi_n(\mathbf{r}) = \langle 0 | \mathcal{O}_{Q\bar{Q}}(\mathbf{r}) | n \rangle \quad (2)$$

with \mathbf{r} -dependent quark-antiquark operator $\mathcal{O}_{Q\bar{Q}}(\mathbf{r})$, where \mathbf{r} is the relative coordinate between a quark (Q) and antiquark (\bar{Q}) at a certain time slice. Although $\mathcal{O}_{Q\bar{Q}}(\mathbf{r})$ can be defined in a gauge-invariant way, we hereafter consider the *Coulomb gauge BS amplitude*. In the Coulomb gauge, the operator is simply given by $\mathcal{O}_{Q\bar{Q}}(\mathbf{r}) = \sum_{\mathbf{x}} \bar{Q}(\mathbf{x}) \Gamma Q(\mathbf{x} + \mathbf{r})$, where Γ represents the Dirac γ metrics. The \mathbf{r} -dependent amplitude, $\phi_n(\mathbf{r})$, in the rest frame is called the *BS wave function*. Therefore, the BS wave function for the n th meson in the rest frame can be determined from the \mathbf{r} -dependent two-point correlation function constructed with a usual quark bilinear

operator \mathcal{O}_α and the \mathbf{r} -dependent one:

$$\begin{aligned} C_\alpha(\mathbf{r}, t) &= \langle 0 | \mathcal{O}_{Q\bar{Q}}(\mathbf{r}, t) \mathcal{O}_\alpha^\dagger(0) | 0 \rangle \\ &= \sum_n \langle 0 | \mathcal{O}_{Q\bar{Q}}(\mathbf{r}) | n \rangle \langle n | \mathcal{O}_\alpha^\dagger | 0 \rangle e^{-tM_n} \\ &= \sum_n \phi_n(\mathbf{r}) V_{n,\alpha}^* e^{-tM_n}, \end{aligned} \quad (3)$$

where M_n is the rest mass of the n th meson, and the \mathbf{r} -dependent amplitude $\phi_n(\mathbf{r})$ corresponds to its BS wave function. The spectral amplitude $V_{n,\alpha}$ defined by $V_{n,\alpha} = \langle 0 | \mathcal{O}_\alpha | n \rangle$ is introduced in the third line of Eq. (3). The correlation function $C_\alpha(\mathbf{r}, t)$ clearly contains a superposition of orthogonal states. The ground-state contribution is indeed isolated from those of the excited states in the large- t region.

Although we only focused on the BS wave function of the ground state in the previous works [13–16], we here intend to obtain the BS wave function of *the radially excited states*. For this purpose, we adopt the variational method [17, 18] to find an optimal meson operator $\mathcal{O}_n^{\text{opt}}$, which solely couples to a specific (n th) state in Eq. (3), since $\langle 0 | \mathcal{O}_n^{\text{opt}} | m \rangle \propto \delta_{n,m}$.

Starting with a set of basis meson operators \mathcal{O}_α ($\alpha = 1, \dots, N$), we consider an $N \times N$ correlation matrix

$$G_{\alpha\beta}(t, 0) = \langle 0 | \mathcal{O}_\alpha(t) \mathcal{O}_\beta^\dagger(0) | 0 \rangle, \quad (4)$$

whose spectral decomposition is given by

$$G_{\alpha\beta}(t, 0) = \sum_n V_{n,\alpha} V_{n,\beta}^* e^{-tM_n} \quad (5)$$

with the spectral amplitude $V_{n,\alpha}$. Next, let us solve the generalized eigenvalue problem,

$$G_{\alpha\beta}(t) \omega_{n,\beta} = \lambda_n(t, t_0) G_{\alpha\beta}(t_0) \omega_{n,\beta}, \quad (6)$$

to obtain the n th eigenvalue $\lambda_n(t, t_0)$, where t_0 is a reference time slice, and its eigenvector is $\omega_{n,\beta}$. If only the N lowest states are propagating in the region where $t \geq t_0$, the n th eigenvalue $\lambda_n(t, t_0)$ is given by a single exponential form, with the rest mass of the n th meson as

$$\lambda_n(t, t_0) = e^{-(t-t_0)M_n}, \quad (7)$$

which corresponds to the eigenvalue of the transfer matrix between two time slices t and t_0 . Details of how to practically compute the eigenvalues $\lambda_n(t, t_0)$ are described in Appendix B of Ref. [19].

Simultaneously, one can obtain its N -dimensional eigenvector $\omega_{n,\alpha}$, which should be orthogonal to the spectral weight $\sum_\alpha \omega_{n,\alpha} V_{m,\alpha}^* = e^{M_n t_0/2} \delta_{n,m}$ [19, 20]. Therefore, the optimal operator can be constructed by an appropriate linear combination of the basis meson operators \mathcal{O}_α with the eigenvector $\omega_{n,\alpha}$:

$$\mathcal{O}_n^{\text{opt}} = \sum_{\alpha=1}^N \omega_{n,\alpha}^* \mathcal{O}_\alpha. \quad (8)$$

The N types of the meson operator with fixed quantum number are, for instance, given by the quark bilinear operators composed of spatially smeared quarks with N different smearing radii. Subsequently, one can obtain the BS wave function of the n th meson state by using N types of \mathbf{r} -dependent two-point correlation functions constructed with the n th eigenvalue λ_n and eigenvector $\omega_{n,\alpha}$ of Eq. (6) as below

$$\phi_n(\mathbf{r}) = e^{M_n(t-t_0/2)} \sum_{\alpha=1}^N \omega_{n,\alpha}^* C_\alpha(\mathbf{r}, t). \quad (9)$$

A similar procedure has been recently applied for a study of the inner structure of glueball states [21].

B. Quark kinetic mass and interquark potential from BS amplitudes

In the past several years, we have demonstrated that the interquark potential and the quark kinetic mass, both of which are key ingredients within the potential description of heavy-heavy and heavy-light mesons, are successfully determined from the BS wave functions of the *ground state* of S -wave charmonium and charm-strange mesons [14–16]. A natural question arises: if we simply apply our proposed method on not only the ground state, but also its excited states, what result comes out, especially from the BS wave function of *radially excited states*?

In this paper, we thus focus on the radially excited states of the S -wave meson states. The Dirac γ matrices (Γ) that appear in both operators $\mathcal{O}_{Q\bar{Q}}(\mathbf{r})$ and \mathcal{O}_α are chosen to be γ_5 for the pseudoscalar (PS) meson ($J^P = 0^-$), and γ_i for the vector (V) meson ($J^P = 1^-$). Recall that the spatial symmetry group on a lattice is reduced to the octahedral point group O_h . To take this into account, the \mathbf{r} -dependent BS wave function $\phi_n(\mathbf{r})$ calculated by Eq. (9) is supposed to be projected in the A_1^+ representation, $\phi_n(\mathbf{r}) \rightarrow \phi_n(A_1^+; r)$, for S -wave mesons. Details of the A_1^+ projection are described in Ref. [15]. Hereafter, the A_1^+ projected BS wave functions of nS states for the PS and V channels are denoted by $\phi_{\text{PS}}^{nS}(r)$ and $\phi_{\text{V}}^{nS}(r)$.

In our preceding studies, the quark kinetic mass m_Q has been read off from the long-distance asymptotic value of the difference of “quantum kinetic energies” (the second spatial derivative of the BS wave function normalized by the BS wave function) between the spin-singlet (PS) and spin-triplet (V) states in the hyperfine multiplet for the $1S$ states [13–16]. We here generalize this idea to nS states. The quark kinetic mass can be determined from a set of the nS wave functions in the following way [13]:

$$m_Q(nS) = \lim_{r \rightarrow \infty} \frac{-1}{E_{\text{hyp}}(nS)} \left\{ \frac{\nabla^2 \phi_{\text{V}}^{nS}(r)}{\phi_{\text{V}}^{nS}(r)} - \frac{\nabla^2 \phi_{\text{PS}}^{nS}(r)}{\phi_{\text{PS}}^{nS}(r)} \right\} \quad (10)$$

with the hyperfine splitting energy of the nS states, $E_{\text{hyp}}(nS) = M_{\text{V}}(nS) - M_{\text{PS}}(nS)$. The derivative ∇^2 that

appears in Eq. (10) is defined by the discrete Laplacian on the lattice. As shown in Ref. [15], a suitable choice of the discrete Laplacian is defined in the discrete polar coordinates in order to reduce the discretization artifacts on the short-range behavior of the interquark potential.

The interquark potential for S -wave states can be decomposed into the central (spin-independent) potential $V_{\text{C}}(r)$ and the spin-spin potential $V_{\text{S}}(r)$, which are defined by the BS wave functions of nS states, $\phi_{\text{PS}}^{nS}(r)$ and $\phi_{\text{V}}^{nS}(r)$, as below:

$$V_{\text{C}}^{nS}(r) = E_{\text{ave}}(nS) + \frac{1}{m_Q(nS)} \left\{ \frac{3}{4} \frac{\nabla^2 \phi_{\text{V}}^{nS}(r)}{\phi_{\text{V}}^{nS}(r)} + \frac{1}{4} \frac{\nabla^2 \phi_{\text{PS}}^{nS}(r)}{\phi_{\text{PS}}^{nS}(r)} \right\} \quad (11)$$

and

$$V_{\text{S}}^{nS}(r) = E_{\text{hyp}}(nS) + \frac{1}{m_Q(nS)} \left\{ \frac{\nabla^2 \phi_{\text{V}}^{nS}(r)}{\phi_{\text{V}}^{nS}(r)} - \frac{\nabla^2 \phi_{\text{PS}}^{nS}(r)}{\phi_{\text{PS}}^{nS}(r)} \right\} \quad (12)$$

where $E_{\text{ave}}(nS) = M_{\text{ave}}(nS) - 2m_Q(nS)$. The mass $M_{\text{ave}}(nS)$ denotes the spin-averaged mass for the nS states as $\frac{3}{4}M_{\text{V}}(nS) + \frac{1}{4}M_{\text{PS}}(nS)$.

C. “Time-dependent” method for the interquark potential

A basic idea of Eqs. (11) and (12) follows the method developed by the HAL QCD Collaboration to derive hadron-hadron interactions from lattice QCD [9, 10]. The original method advocated by the HAL QCD Collaboration starts from the fact that the equal-time BS wave function satisfies the “stationary” Schrödinger equation with a nonlocal and energy-independent potential below the inelastic threshold [10]. We simply apply this method to the quark-antiquark ($Q\bar{Q}$) system [35]. Strictly speaking, no explicit energy dependence of the nonlocal potential in a finite box was proved only for the case of the short-range interaction [10]. In this sense, the $Q\bar{Q}$ system, where confining quark interaction is long ranged, does not guarantee the existence of an energy-independent nonlocal potential even below open heavy-flavor thresholds.

Thus, assuming the existence of an energy-independent nonlocal potential in the $Q\bar{Q}$ system [36], let us consider the following “time-independent” Schrödinger equation for the BS wave function ϕ_Γ in the nonrelativistic approximation:

$$\left\{ E_\Gamma + \frac{\nabla^2}{m_Q} \right\} \phi_\Gamma(\mathbf{r}) = \int d\mathbf{r}' U(\mathbf{r}, \mathbf{r}') \phi_\Gamma(\mathbf{r}'), \quad (13)$$

where $E_\Gamma = M_\Gamma - 2m_Q$. As discussed in Refs [13, 14], for the S -wave meson states, the local potentials $V_{\text{PS}}(r)$ and $V_{\text{V}}(r)$ defined at the leading order of the velocity expansion, $U(\mathbf{r}, \mathbf{r}') = \{V_{\text{PS(V)}}(r) + \mathcal{O}(v^2)\} \delta^2(\mathbf{r} - \mathbf{r}')$ with

$v = |\nabla/m_Q|$, are given by

$$V_{\text{PS(V)}}(r) = E_{\text{PS(V)}} + \frac{1}{m_Q} \frac{\nabla^2 \phi_{\text{PS(V)}}(r)}{\phi_{\text{PS(V)}}(r)}. \quad (14)$$

The interquark potential $V_{\text{PS(V)}}(r)$ can be written by $V_{\text{PS(V)}}(r) = V_C(r) + (\mathbf{S}_Q \cdot \mathbf{S}_{\bar{Q}}) V_S(r)$, where the spin operator $\mathbf{S}_Q \cdot \mathbf{S}_{\bar{Q}}$ may be replaced by an expectation value of $-3/4$ ($1/4$) for the PS(V) state. Then, $V_C(r)$ and $V_S(r)$ are separately obtained, as shown in Eqs. (11) and (12).

In our preceding works [13–16], the central and spin-spin interquark potentials are successfully extracted from the $1S$ meson states by using this method. We then use resulting potentials and quark masses as purely theoretical inputs so as to solve the nonrelativistic Schrödinger equation for calculating accessible energy levels of charmonium and charmed-strange mesons without unknown parameters. The resultant spectra below the $D\bar{D}$ and DK thresholds excellently agree with well-established ex-

perimental data [16].

Starting with no explicit energy dependence on the nonlocal potential, the HAL QCD Collaboration has proposed an alternative method to derive the hadron-hadron interactions by a so-called “time-dependent” Schrödinger-like equation [23], instead of Eq. (13). Here, we also may apply the new method to our $Q\bar{Q}$ system of interest. For this purpose, let us introduce the following correlation function:

$$R_\Gamma(\mathbf{r}, t) = C_\Gamma(\mathbf{r}, t)/(e^{-m_Q t})^2, \quad (15)$$

where m_Q denotes the quark kinetic mass that should be determined in advance, as described in Eq. (10).

Considering the time derivative, $\frac{\partial}{\partial t} R_\Gamma(\mathbf{r}, t)$, with the help of the spectral decomposition of the original \mathbf{r} -dependent correlation function $C_\Gamma(\mathbf{r}, t)$, we then arrive at the time-dependent Schrödinger-like equation for the $Q\bar{Q}$ system [23] as well:

$$\left\{ \frac{1}{4m_Q} \frac{\partial^2}{\partial t^2} - \frac{\partial}{\partial t} + \frac{\nabla^2}{m_Q} \right\} R_{\text{PS(V)}}(\mathbf{r}, t) = \int d\mathbf{r}' U(\mathbf{r}, \mathbf{r}') R_{\text{PS(V)}}(\mathbf{r}', t), \quad (16)$$

where the first term on the left-hand side is responsible for the fully relativistic treatment for the kinetic term. For the S -wave mesons, the A_1^+ projection is supposed to be applied to the correlation functions defined above as $R_{\text{PS(V)}}(\mathbf{r}, t) \rightarrow R_{\text{PS(V)}}(A_1^+; r, t)$. Starting from Eq. (16) with the same approximation on the nonlocal potential $U(\mathbf{r}, \mathbf{r}')$, we thus obtain the alternative formula of $V_{\text{PS(V)}}(r)$ as follows:

$$V_{\text{PS(V)}}(r) = \frac{1}{m_Q} \frac{\nabla^2 R_{\text{PS(V)}}(r, t)}{R_{\text{PS(V)}}(r, t)} - \frac{(\partial/\partial t) R_{\text{PS(V)}}(r, t)}{R_{\text{PS(V)}}(r, t)} + \frac{1}{4m_Q} \frac{(\partial/\partial t)^2 R_{\text{PS(V)}}(r, t)}{R_{\text{PS(V)}}(r, t)}. \quad (17)$$

We hereafter will omit the second derivative term of t in the analysis, treating it on the same footing as was done in Eq. (13). Details of this relativistic correction will be discussed in a separate publication [24].

The most important feature of the time-dependent approach is that “single-state dominance” is not necessarily achieved in the given correlation function $R_\Gamma(r, t)$ [23]. Therefore, it enables us to use the data of $R_\Gamma(r, t)$ in the earlier time range, within the condition that the inelastic contribution is negligible in the entire t region analyzed. This advantage may lead to small statistical and systematic uncertainties on the final result.

There is one caveat: the new method for the $Q\bar{Q}$ system highly assumes that a series of the BS wave functions from the ground state to excited states is generated by the same “nonlocal” potential. In this work, we will

later verify the validity of this method in the $Q\bar{Q}$ system through a direct comparison of the interquark potentials defined in Eqs. (11) and (12), which are independently determined from the BS wave functions of both the $1S$ and $2S$ charmonium states.

III. NUMERICAL RESULTS

The computation of the BS wave functions for the charmonium system is carried out on a lattice, $N_s^3 \times N_t = 32^3 \times 64$ using the (2+1)-flavor PACS-CS gauge configurations, where the simulated pion mass is closest to the physical point as $m_\pi = 156(7)$ MeV [25]. Simulation parameters of PACS-CS gauge configurations are summarized in Table I. Our results are analyzed on all 198 gauge configurations, which are available through International Lattice Data Grid and the Japan Lattice Data Grid [37].

For the charm quark, we employ the relativistic heavy quark (RHQ) action that removes the main discretization errors induced by large charm quark mass. The RHQ action, which is a variant of the Fermilab approach [26], is the anisotropic version of the $\mathcal{O}(a)$ improved Wilson action with five parameters κ_c , ν , r_s , c_B , and c_E , called *RHQ parameters* (for more details, see Refs. [27, 28]).

The parameters r_s , c_B , and c_E in the RHQ action are determined by tadpole improved one-loop perturbation theory [28] with a reference of the $\mathcal{O}(a)$ improvement coefficient, $c_{\text{SW}} = 1.715$ for light quarks [25]. As for

TABLE I: Parameters of (2+1)-flavor dynamical QCD gauge field configurations generated by the PACS-CS Collaboration [25]. The columns list the number of flavors, the lattice volume, the β value, hopping parameters for light and strange quarks, approximate lattice spacing (lattice cutoff), spatial physical volume, pion mass, and the number of configurations to be analyzed.

N_f	$N_s^3 \times N_t$	β	κ_{ud}	κ_s	a [fm] (a^{-1} [GeV])	$N_s a$ [fm]	M_π [MeV]	No. of configurations
2 + 1	$32^3 \times 64$	1.9	0.13781	0.13640	0.0907(13) (≈ 2.18)	2.90(4)	≈ 156	198

ν , we use a nonperturbatively determined value, which is tuned by reproducing the effective speed of light as unity in the dispersion relation for the spin-averaged $1S$ -charmonium state, since the parameter ν is sensitive to the size of hyperfine splitting energy [29]. Our chosen RHQ parameters are summarized in Table II.

When the quark propagator is computed, Dirichlet boundary conditions are imposed for the time direction at $t/a = 0$ and 63 to eliminate unwanted contributions across time boundaries. Source location is set at two different time slices, $t_s/a = 6$ and 57, both of which are the same distance away from two boundaries, so as to avoid the temporal boundary effect. Averaging the results of calculations over multiple sources would help to reduce the statistical uncertainties. Instead of changing the places of the boundaries and source locations, a temporal shift can be applied to the gauge configurations $\{U_\mu(\mathbf{x}, t)\} \rightarrow \{U_\mu(\mathbf{x}, t + t_{\text{shift}})\}$ due to the temporal periodicity of the lattice.

We use gauge-covariant, approximately Gaussian-shaped smearing [30, 31] for constructing the spatially smeared operator $\mathcal{O}_\alpha(x) = \bar{Q}_\alpha(x)\Gamma Q_\alpha(x)$ with

$$Q_\alpha(\mathbf{x}, t) = \left(1 + \frac{W_G^2}{4N_G} \mathbf{D}^2\right)^{N_G} Q(\mathbf{x}, t), \quad (18)$$

where \mathbf{D}^2 denotes the covariant lattice Laplacian, and α labels a set of two parameters as $\alpha = \{N_G, W_G\}$ [32]. Here, N_G is the number of times the smearing kernel acts on the quark fields, while W_G is the width of the Gaussian that results in $N_G \rightarrow \infty$. We adopt four parameter sets: $\{N_G, W_G\} = \{10, 1.0\}$, $\{15, 2.0\}$, $\{20, 3.0\}$, and $\{30, 4.0\}$, so as to construct the 4×4 correlation matrix defined in Eq. (4) and also four types of \mathbf{r} -dependent two-point correlation function, defined in Eq. (3).

For a single-parameter set, we compute 32 valence quark propagators per gauge configuration with eight different spatial centers of the Gaussian sources, which are located at the corners of a 16^3 cube, on two different time slices $t_s/a = 6$ and 57, using two different temporal shifts $t_{\text{shift}}/a = 0$ and 32, so as to increase statistics. All 32 sets of usual and \mathbf{r} -dependent two-point correla-

TABLE II: The hopping parameter κ_c and the RHQ parameters (ν , r_s , c_B , and c_E) used for the charm quark.

κ_c	ν	r_s	c_B	c_E
0.10819	1.2153	1.2131	2.0268	1.7911

tion functions are folded together to create the single-correlation functions as a function of t' defined in the range $0 \leq t'/a \leq 57$. Hereafter, t' is simply denoted as t .

Let us first present the effective masses of the S -wave charmonium (η_c and ψ) states in the variational method. An effective mass is defined as

$$M_{n,\Gamma}(t) = \log \frac{\lambda_{n,\Gamma}(t, t_0)}{\lambda_{n,\Gamma}(t+a, t_0)}, \quad (19)$$

where $\lambda_{n,\Gamma}(t, t_0)$ is the n th eigenvalue of the 4×4 correlation matrix for $\Gamma = \text{PS}$ or V . In this study, we choose the reference time slice as $t_0/a = 3$, where the resulting mass is less sensitive to variation of t_0 .

TABLE III: Masses of S -wave charmonium states calculated from eigenvalues of the 4×4 transfer matrix up to $3S$ states. The fitting ranges and values of $\chi^2/\text{d.o.f.}$ are also included. For $1S$ and $2S$ charmonium states, the spin-averaged mass (M_{ave}) and hyperfine splitting energy (E_{hyp}) are also evaluated. Results are given in units of GeV.

State	J^{PC}	Fit range	Mass [GeV]	$\chi^2/\text{d.o.f.}$
$\eta_c(1S)$	0^{-+}	[33:47]	2.9850(5)	1.08
$\eta_c(2S)$	0^{-+}	[4:17]	3.729(15)	0.80
$\eta_c(3S)$	0^{-+}	[4:11]	4.553(34)	0.77
J/ψ	1^{-+}	[33:47]	3.0986(14)	1.21
$\psi(2S)$	1^{-+}	[4:17]	3.801(16)	1.05
$\psi(3S)$	1^{-+}	[4:11]	4.679(34)	1.53
$M_{\text{ave}}(1S)$	3.0702(11)	...
$M_{\text{ave}}(2S)$	3.783(15)	...
$E_{\text{hyp}}(1S)$	0.1135(12)	...
$E_{\text{hyp}}(2S)$	0.0725(56)	...

Figure 1 shows the effective mass plots of the first three eigenvalues $\lambda_{1,\Gamma} > \lambda_{2,\Gamma} > \lambda_{3,\Gamma}$ for the PS and V channels. Here, we remark that $\lambda_{n,\text{PS(V)}}$ is associated with the nS state. The variational method with the correlation matrix constructed in our chosen basis successfully separates the first excited ($2S$) state and the second excited ($3S$) state from the ground ($1S$) state.

The horizontal solid lines represent each fit result with its 1 standard deviation obtained by a covariant single exponential fit. In Table III, we summarize the results of masses of the three lowest-lying S -wave charmonium states together with fit ranges used in the fits and values of χ^2 per degrees of freedom (d.o.f.).

The fit results for $3S$ states are rather sensitive to the choice of the fit range, since the signal of the $3S$ states

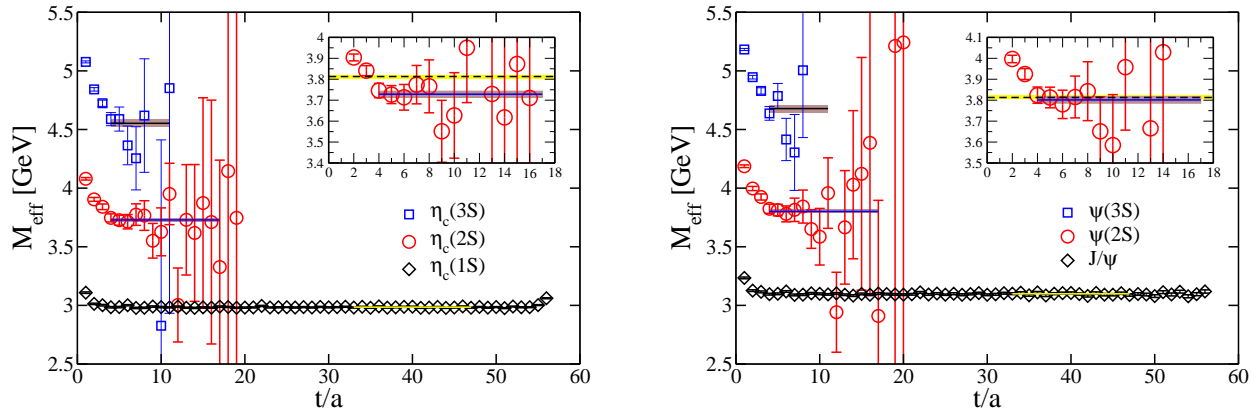


FIG. 1: Effective mass plots for the $\eta_c(nS)$ (left panel) and $\psi(nS)$ (right panel) states. Charmonium states are specified in the legend. Solid lines indicate fit results, and shaded bands display the fitting ranges and 1 standard deviation. The inset in each panel shows a magnified view of the effective mass of the 2S state together with the P -wave $D\bar{D}$ threshold (dashed line).

dies out quickly; therefore, those values involved in Table III are just listed for reference. The errors quoted in all of the results represent only the statistical errors given by the jackknife analysis.

For the 1S states, all results including M_{ave} and E_{hyp} obtained in the variational method are fully consistent with our previous study, where the charm quark propagators were computed by the wall source with the Coulomb gauge fixing [16]. It is worth recalling that the values of κ_c and ν in the RHQ parameters are chosen to reproduce both the experimental spin-averaged mass and hyperfine splitting energy of 1S charmonium states. This is the reason why our results of the 1S states are very close to the experimental values.

On the other hand, the masses of the 2S states correspond to the theoretical predictions from dynamical lattice QCD. We obtain results of $M_{\eta_c(2S)} = 3.729(15)(21)$ GeV and $M_{\psi(2S)} = 3.801(16)(31)$ GeV. The first errors are statistical, and the second errors are systematic uncertainties due to variations of t_{min} in the fit range $[t_{\text{min}}/a : t_{\text{max}}/a]$.

Although those values are about 100 MeV higher than the experimental values of $M_{\eta_c(2S)}^{\text{exp}} = 3.639$ GeV and $M_{\psi(2S)}^{\text{exp}} = 3.686$ GeV, similarly higher values are reported in Ref. [33]. In addition, the hyperfine splitting energy of the 2S states is $M_{\psi(2S)} - M_{\eta_c(2S)} = 73(6)(1)$ MeV, of which the value is slightly larger than the experimental value of 47 MeV. Needless to say, the higher-lying states might suffer much from the lattice artifacts—finite size and lattice discretization effects—compared to their ground state [38].

Our results for the $\eta_c(2S)$ and $\psi(2S)$ masses are near to and slightly above the experimental value of the $D\bar{D}$ threshold energy (~ 3.730 GeV). We, however, remark that since the η_c and ψ mesons have negative parity, the

P -wave $D\bar{D}$ threshold energy, which is defined as the total energy of the noninteracting $D\bar{D}$ state with the smallest nonzero momentum $|\mathbf{p}_{\text{min}}| = 2\pi/(La)$, is appropriate for comparison with the $\eta_c(2S)$ and $\psi(2S)$ masses [34]. In our calculation, the lowest open charm threshold is 3.813(8) GeV, which is determined with the measured D -meson mass [$M_D = 1.858(4)$ GeV]. Our result for the $\psi(2S)$ mass is slightly below but close to the P -wave $D\bar{D}$ threshold, while the $\eta_c(2S)$ mass is well below the P -wave $D\bar{D}$ threshold [39]. In this context, it would be important to know how much the $D\bar{D}$ mixing effect has affected the spectroscopy of the 2S charmonium states.

Although more systematic study is thus necessary for the spectroscopy of the radially excited states, it is beyond the scope of this paper. Rather, our main purpose is practically to get the optimal charmonium operators for both 1S and 2S states using the resulting eigenvectors $(\omega_{n,\Gamma})_\alpha$ of the transfer matrix in the variational method. As a result, the BS wave functions for 1S and 2S states are obtained through Eq. (9) separately.

In Fig. 2, we show the reduced wave functions $u_{n,\Gamma}(\mathbf{r}) = r\phi_{n,\Gamma}(\mathbf{r})$ of both 1S and 2S charmonium states for displaying the spatial distribution of the BS wave function. The wave functions displayed in Fig. 2 are normalized as $\sum_{\mathbf{r}} |\phi_{n,\Gamma}(\mathbf{r})|^2 = 1$ [40]. We plot data points taken along simpler \mathbf{r} vectors, which are multiples of three directions—(1,0,0), (1,1,0), and (1,1,1)—in order to avoid large discretization errors induced by the discrete Laplacian ∇^2 [15] in later discussion.

Compared with the results of 1S states, the BS wave functions of both $\eta_c(2S)$ and $\psi(2S)$ states exhibit a specific nodal structure in the radial direction, as we expected. Although at first glance the 2S wave functions are slightly extended in space in comparison to the 1S wave functions, the spacial lattice extent $N_s a \approx 2.9$ fm is likely to be large enough to study even the 2S char-

monium system as well as the ground-state charmonium states.

The wave function provides information about a spatial size of the charmonium meson as the root-mean-square (rms) radius r_{rms} , which can be determined by

$$r_{\text{rms}}^2 = \frac{\sum_{\mathbf{r}} r^2 |\phi_{n,\Gamma}(\mathbf{r})|^2}{\sum_{\mathbf{r}} |\phi_{n,\Gamma}(\mathbf{r})|^2} = \frac{\int dr r^2 |u_{n,\Gamma}(r)|^2}{\int dr |u_{n,\Gamma}(r)|^2}. \quad (20)$$

We then obtain the smaller rms radii for $1S$ states as $(r_{\text{rms}})_{\overline{1S}} \sim 0.38$ fm, while $2S$ states yield comparatively larger values as $(r_{\text{rms}})_{\overline{2S}} \sim 0.60$ fm. Another important aspect of the resulting r_{rms} is that both the $1S$ and $2S$ states satisfy the relation $r_{\text{rms,PS}} < r_{\text{rms,V}}$. This simply indicates the repulsive nature of spin-spin interaction near the origin for the higher spin states. All results of r_{rms} are summarized in Table IV.

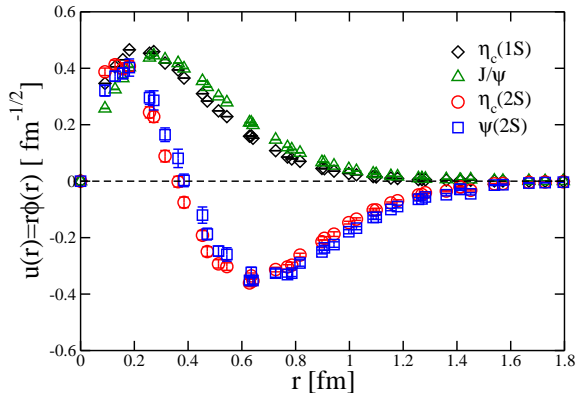


FIG. 2: The reduced BS wave functions $u(r) = r\phi(r)$ for the $\eta_c(1S)$ (diamonds), J/ψ (triangles), $\eta_c(2S)$ (circles), and $\psi(2S)$ (squares) states, shown as functions of the spatial distance r . They are normalized as $\sum_{\mathbf{r}} |\phi(\mathbf{r})|^2 = 1$. The time average was performed in the range of $[t_{\text{min}}/a : t_{\text{max}}/a] = [24 : 33]$ for the $1S$ states and $[7:12]$ for the $2S$ states.

We also verify the orthonormality condition between the resulting $1S$ and $2S$ wave functions through the following overlap (OVL) coefficient:

$$C_{\text{OVL}} = \frac{\sum_{\mathbf{r}} \phi_{\Gamma}^{1S}(\mathbf{r}) \phi_{\Gamma}^{2S}(\mathbf{r})}{\sqrt{\sum_{\mathbf{r}} |\phi_{\Gamma}^{1S}(\mathbf{r})|^2} \sqrt{\sum_{\mathbf{r}} |\phi_{\Gamma}^{2S}(\mathbf{r})|^2}}. \quad (21)$$

We then obtain $|C_{\text{OVL}}| = 0.174(46)(3)$ for the PS channel and $|C_{\text{OVL}}| = 0.101(52)(6)$ for the V channel. The first error is statistical, and the second one is systematic uncertainty due to the choice of the numerical integral methods in r space. Nonzero values of $|C_{\text{OVL}}|$ in both the PS and V channels suggest that the $2S$ wave function may receive non-negligible contamination of the $1S$ state from an unknown origin.

There is, however, a hint from Fig. 1. Around $t/a = 8$, the signal of the $2S$ states in the effective mass plot be-

comes noisy, and the isolation of the $2S$ states is statistically insignificant due to the large uncertainties. Even if the eigenvector for the $2S$ states, $\omega_{2S,\alpha}$, is properly calculated in the variational method, contributions of the $2S$ state in the correlation $C_{\alpha}(\mathbf{r}, t)$ are exponentially suppressed by its large mass $M_{2S} (> M_{1S})$ as a function of t . Therefore, if we include the data points of the $2S$ wave function determined at the larger t during the averaging process over the time-slice range, the resulting $2S$ wave function may receive a little component of the $1S$ wave function that is caused by incomplete orthogonal factorization within numerical precision and its enhancement due to the relative suppression of the $2S$ -state contribution in the large- t region. Indeed, we observe that the overlap coefficient gets away from zero as the value of t_{min} increases in the time-averaged procedure.

The small but nonzero value of $|C_{\text{OVL}}|$ may cause serious systematic error in the early estimation of the rms radii for $2S$ states. Taking into account such contaminations in the resulting $2S$ wave functions, we perform the Gram-Schmidt orthonormalization (GSO) so as to get an exactly orthogonal wave function to the $1S$ state as

$$\tilde{\phi}_{\Gamma}^{2S}(\mathbf{r}) = \frac{\phi_{\Gamma}^{2S}(\mathbf{r})}{\sqrt{\sum_{\mathbf{r}} |\phi_{\Gamma}^{2S}(\mathbf{r})|^2}} - C_{\text{OVL}} \times \frac{\phi_{\Gamma}^{1S}(\mathbf{r})}{\sqrt{\sum_{\mathbf{r}} |\phi_{\Gamma}^{1S}(\mathbf{r})|^2}}. \quad (22)$$

We then recalculate the rms radii of the $2S$ states with the above modified $2S$ wave function $\tilde{\phi}_{\Gamma}^{2S}(\mathbf{r})$ for each channel. We obtain slightly larger values as $(r_{\text{rms}})_{\overline{2S},\text{GSO}} \sim 0.63$ fm in comparison to the ones obtained from the original $2S$ wave functions. The modified results of r_{rms} for $2S$ states are also included in Table IV.

In the following discussions, we do not use the modified $2S$ wave functions and keep the original ones for our later analysis, since there is only a slight difference in their profile shapes, which mainly appears at short distances, between the $2S$ wave functions obtained before and after the Gram-Schmidt orthonormalization.

TABLE IV: Summary of the rms radii of $1S$ and $2S$ charmonium states, which are evaluated from the BS wave functions on the lattice. Results are given in units of fm. ‘‘Raw’’ and ‘‘GSO’’ stand for results obtained before and after the Gram-Schmidt orthonormalization.

State	$\eta_c(1S)$	J/ψ	$\eta_c(2S)$	$\psi(2S)$
r_{rms} [fm] (Raw)	0.3348(2)	0.3885(6)	0.563(14)	0.612(18)
r_{rms} [fm] (GSO)	0.606(4)	0.636(7)

As described in Sec. IIB, the BS wave function for mesons can provide more profound information about the internal structure of the quark-antiquark bound states. We first discuss the quark kinetic mass, which can be read off from the difference of ‘‘quantum kinetic energies’’ $\nabla^2 \phi_{\Gamma} / \phi_{\Gamma}$ between the members of hyperfine multiplets, as was shown in Eq. (10). The time average for $\nabla^2 \phi_{\Gamma} / \phi_{\Gamma}$ appearing in Eq. (10) was performed in the

range of $[t_{\min}/a : t_{\max}/a] = [24 : 33]$ for the $1S$ states and $[7:12]$ for the $2S$ states.

Figure 3 shows that asymptotic constants obtained from the right-hand side of Eq. (10) for both $1S$ and $2S$ states appear to be overlapped in the range of $0.6 \text{ fm} \lesssim r \lesssim 1.0 \text{ fm}$. A value of the kinetic mass of the charm quark is determined by a constant fit over above the r -range with $\chi^2/\text{d.o.f.} < 2$.

We then obtain $m_Q(1S) = 1.816(21) \text{ GeV}$ from the $1S$ wave functions and $m_Q(2S) = 1.847(145) \text{ GeV}$ from the $2S$ wave functions. Both values are consistent with each other, and also with our previous work as listed in Table V. This indicates that within the current precision, a unique result for the quark kinetic mass is likely given regardless of the choice of either the ground- or excited-state pairs. This observation is highly consistent with the success of a potential description of the charmonium system.

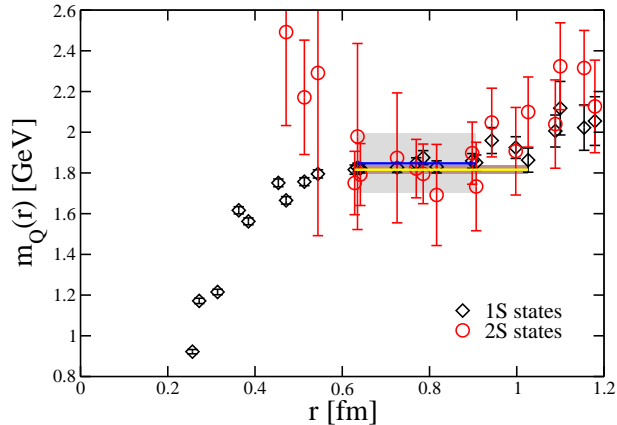


FIG. 3: The determination of quark kinetic mass within the BS amplitude method. Horizontal solid lines indicate a value of quark kinetic mass obtained by fitting an asymptotic constant obtained from either $1S$ or $2S$ states. Shaded bands indicate the fitting range and a statistical error estimated by the jackknife method.

We are now ready to consider the final question of whether or not a series of the BS wave functions from the ground state to excited states is generated by the same “nonlocal” potential. To answer this question is meant to justify the time-dependent BS amplitude method even for the $Q\bar{Q}$ system.

In order to perform rigorous comparison, we will determine the central spin-independent part of the interquark potential $V_C(r)$ from the BS wave functions of excited states in a manner independent from those of ground states. Indeed, the quark kinetic masses have been already evaluated for both $1S$ and $2S$ states. Therefore, the central potential $V_C(r)$ and the quark mass m_Q can be self-consistently determined within a single set of r -

dependent two-point correlation functions for each nS state, as shown in Eq. (11).

TABLE V: Summary of charm quark masses, which are determined from the BS amplitudes of both $1S$ and $2S$ charmonium states. Their fit ranges $[r_{\min}/a : r_{\max}/a]$ are summarized in units of GeV.

Method	Previous work [16]	Variational method	
Type of source	Wall source	Gauss-smearred sources	
State	$1S$	$1S$	$2S$
m_Q [GeV]	1.784(23)	1.816(21)	1.847(145)
Fit range	$[6 : 7\sqrt{3}]$	$[4\sqrt{3} : 8\sqrt{2}]$	$[7 : 10]$

Figure 4 shows two independent results of the central potential $V_C(r)$ using the BS wave functions of either $1S$ or $2S$ states. For clarity of the figure, the “threshold energy value” $2m_Q$, which is a part of the constant energy shift ($E_{\text{ave}} = M_{\text{ave}} - 2m_Q$), is not subtracted. The spin-averaged masses, $M_{\text{ave}}(1S)$ and $M_{\text{ave}}(2S)$, have been obtained by the variational method as described previously. Thus, it should be emphasized that no adjustment constant is added for comparison.

The gross features of the resulting central potential $V_C^{2S}(r)$ from the $2S$ states are basically analogous to those of the $1S$ states $V_C^{1S}(r)$. Although data points in the intermediate ($0.5 \lesssim r \lesssim 1.1 \text{ fm}$) and short-range ($r \lesssim 0.3 \text{ fm}$) parts of the $V_C^{2S}(r)$ agree well with a shape of $V_C^{1S}(r)$, some discrepancy beyond the quoted statistical errors appears in two specific regions: around $r = 0.4 \text{ fm}$ and at long distances ($r \gtrsim 1.1 \text{ fm}$).

The origin of the former discrepancy can be attributed to the presence of a node in the $2S$ wave function, which is located at $r \approx 0.4 \text{ fm}$, as shown in Fig. 2. One should be reminded that the potential defined in the BS amplitude method is basically calculated by the second spatial derivative of the BS wave function divided by the BS wave function, $\nabla^2 \phi_\Gamma / \phi_\Gamma$. Therefore, the potential cannot be given only at nodes of the BS wave function.

In this sense, the statistical uncertainties may lead to divergent behavior near the nodes. For the $2S$ wave functions, the resulting potential is rendered positively (negatively) divergent on the left (right) side of its singularity. This accounts for a discontinuity behavior appearing in $V_C^{2S}(r)$. Another consequence of the presence of the nodes may enhance a chance of unwanted excited-state contamination, since the strength of other state contributions in r -dependent two-point correlation functions may exceed that of the target state at its nodes.

As for another discrepancy found at long distances, it should be simply because of the larger statistical uncertainties in the BS wave function of the higher-lying excited states. As shown in Fig. 2, the BS wave functions of both $1S$ and $2S$ states are localized around the origin and vanish at long distances. The signal-to-noise ratio on the quantity of $\nabla^2 \phi_\Gamma / \phi_\Gamma$ becomes worse rapidly as the spatial distance r increases because of the localized

nature of the BS wave functions. This tends to cause large systematic uncertainties at long distances, stemming from the choice of time window for the averaging process of $\nabla^2\phi_\Gamma/\phi_\Gamma$ over the time-slice range (for details on the “time-average” procedure, see Ref. [15]). The time average for $\nabla^2\phi_\Gamma/\phi_\Gamma$ was performed in the range of $[t_{\min}/a : t_{\max}/a] = [24 : 33]$ for the $1S$ states and $[7:12]$ for the $2S$ states.

Indeed, the *string-breaking-like* behavior of the charmonium potentials found in our previous study [16] has, as expected, gone away in $V_C^{1S}(r)$, whose statistical uncertainties at long distances are much under control in this study, due to effectively higher statistics using the average of multiple sources. We then conclude that the discrepancies of $V_C^{1S}(r)$ and $V_C^{2S}(r)$ appearing in two regions are highly associated with statistical issues on the quantity of $\nabla^2\phi_\Gamma/\phi_\Gamma$, particularly for the $2S$ states. In other words, the standard errors of $V_C^{2S}(r)$ displayed in Fig. 4 tend to be underestimated in those regions, where the systematic uncertainties should be seriously taken into account.

To settle the above issues, we decide to utilize the time-dependent method only for the analysis of $V_C^{2S}(r)$, since it enables us to use the data of the $2S$ states in the earlier time range, where the statistical uncertainties are relatively under control. It is then expected to suppress the signal-to-noise ratio on $V_C^{2S}(r)$, and also to reduce the hidden systematic uncertainties stemming from a slight contamination of the $1S$ state during the averaging process over the time-slice range as we discussed before. Here, we note that this limited usage of the time-dependent method *does not assume* that the BS wave functions of the $1S$ and $2S$ states are generated by the same potential. We rather assume that the third energy levels disentangled by the variational method in this study are associated with the $3S$ states. In addition, the nonlocal potential that generates the $3S$ states is identical to that of the $2S$ states.

In Fig. 5, we show a comparison between $V_C^{1S}(r)$ from the time-independent method and $V_C^{2S}(r)$ from the time-dependent method. It again should be emphasized that no adjustment constant is added for comparison. In the determination of $V_C^{2S}(r)$, a change from the time-independent method to the time-dependent method allows us to use the data in the earlier time range. As a result, the time-average procedure was performed in the range of $[t_{\min}/a : t_{\max}/a] = [5 : 11]$, which contains data points of the correlation $C_\alpha(\mathbf{r}, t)$ at $t/a = 4$ nearest to the reference time ($t_0/a = 3$). Recall that there are the derivative terms of t in the time-dependent method.

The new result of $V_C^{2S}(r)$ using the time-dependent method fairly agrees with $V_C^{1S}(r)$. Although a remnant of the discontinuity behavior near the node of the BS wave functions of the $2S$ states remains visible, the resulting charmonium potential $V_C^{2S}(r)$ exhibits linearly rising potential at large distances and Coulomb-like potential at short distances, and is identical to $V_C^{1S}(r)$ within the current statistical precision.

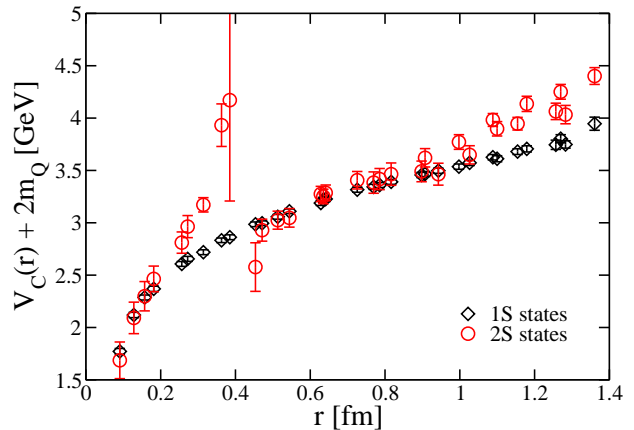


FIG. 4: Central (spin-independent) charmonium potentials calculated from the BS wave functions using the S -wave ground ($1S$) states and their first radially excited ($2S$) states. For clarity of the figure, the “threshold energy value” $2m_Q$, that was encoded in the constant energy shift ($E_{\text{ave}}^{nS} = M_{\text{ave}}^{nS} - 2m_Q$), is not subtracted. Note that there is no adjustment parameter.

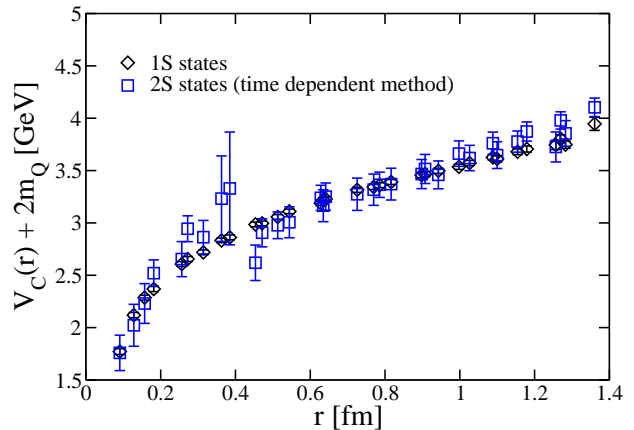


FIG. 5: Central (spin-independent) charmonium potentials from the time-independent method for $1S$ states and the time-dependent method for $2S$ states. Note that there is no adjustment parameter, the same as in Fig. 4.

Finally, we also determine the spin-spin potential from the BS wave functions of both $1S$ and $2S$ states. In Fig. 6, we compile three results of the spin-spin charmonium potential. Open diamond symbols represent results of the spin-spin potential from the $1S$ states, $V_S^{1S}(r)$, while results from both the time-independent (circles) and time-dependent (squares) methods are displayed for the spin-spin potential from the $2S$ states, $V_S^{2S}(r)$.

The potential $V_S^{1S}(r)$ exhibits a repulsive interaction

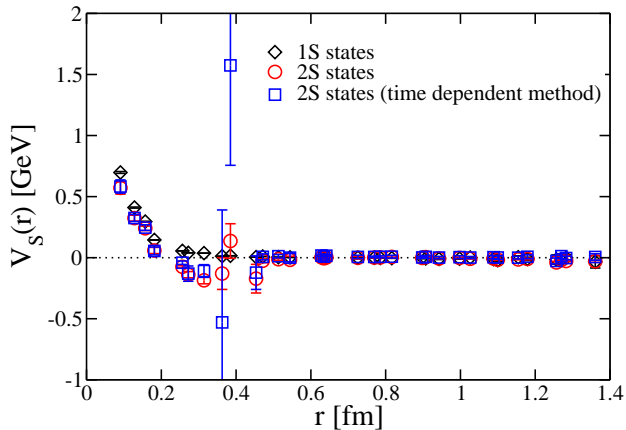


FIG. 6: Spin-spin charmonium potentials from the time-independent method for both $1S$ states (diamonds) and $2S$ states (circles), and also from the time-dependent method for $2S$ states (squares).

for spin-triplet states and an attractive interaction for spin-singlet states with a finite range of $r \lesssim 0.6$ fm, which is the same as that discussed in Refs [14, 16]. On the other hand, the circle symbols of the potential $V_S^{2S}(r)$, which are given by the original time-independent method, reveal a small negative dip in the region $0.3 \lesssim r \lesssim 0.4$ fm, though the positive part of $V_S^{2S}(r)$ at short distances should be the dominant contribution of the finite-range spin-spin interaction.

The presence of the small negative dip makes a small difference between $V_S^{1S}(r)$ and $V_S^{2S}(r)$ within the time-independent approach. However, the dip location is apparently near the node of the $2S$ wave functions. As described previously, there is a subtlety in the calculation of $\nabla^2 \phi_\Gamma / \phi_\Gamma$ near the zero of ϕ_Γ . Thus, in the case of the spin-independent central potential, it is found that an application of the time-dependent method is certainly effective in the analysis of the $2S$ states.

Although there was no drastic change from the time-independent method to the time-dependent method in the case of the spin-spin potential, the latter result slightly becomes in agreement with $V_S^{1S}(r)$ within a few standard deviations. We may conclude that the difference between $V_S^{1S}(r)$ and $V_S^{2S}(r)$ is not statistically significant. We do not, however, rule out the possibility that different sizes of the S - D mixing effect on the J/ψ and $\psi(2S)$ states may lead to some difference in the spin-spin potential.

Indeed, the present calculation does not take into account the presence of the tensor interaction in the spin-dependent potentials, which causes possible partial-wave mixings except for the PS channel. No significant difference found in both the central and spin-spin potentials calculated from the $1S$ and $2S$ states suggests that the

possible S - D mixing is not a leading effect for both the J/ψ and $\psi(2S)$ states.

IV. SUMMARY

We have calculated the BS wave functions for both the ground and first excited states of the S -wave charmonia (η_c and ψ mesons) in full lattice QCD. Our simulations have been carried out with the RHQ action for the charm quark ($M_{\eta_c} \approx 2985$ MeV and $M_{J/\psi} \approx 3099$ MeV) on the (2+1)-flavor PACS-CS gauge configurations near the physical point ($M_\pi \approx 156$ MeV).

The optimal charmonium operators have been successfully obtained for the ground and first excited states of the S -wave charmonia, using the variational method by means of a set of basis meson operators that are composed of spatially smeared quark sources with four successive smearing radii. We then calculated the BS wave functions of both the $1S$ and $2S$ charmonium states. Compared with the results of $1S$ states, the BS wave functions of both the $\eta_c(2S)$ and $\psi(2S)$ states exhibit a specific nodal structure in the radial direction.

Although the orthonormality condition is slightly violated between the resulting $1S$ and $2S$ wave functions, there is only a slight difference in the profile shapes between the $2S$ wave functions obtained before and after the Gram-Schmidt orthonormalization (GSO). In either case, it is observed that the $2S$ wave functions $\phi_\Gamma^{2S}(r)$ are slightly extended in space in comparison to the $1S$ wave functions $\phi_\Gamma^{1S}(r)$. Indeed, we obtain a relatively larger spin-averaged value of $(r_{\text{rms}})_{\overline{2S}} \sim 0.60$ fm (before GSO) and 0.63 fm (after GSO) for the $2S$ states in comparison to that of the $1S$ states, $(r_{\text{rms}})_{\overline{1S}} \sim 0.38$ fm.

We have read off the value of the charm quark mass from the long-distance asymptotic value of the difference of “quantum kinetic energies,” $\nabla^2 \phi_\Gamma / \phi_\Gamma$, between the members of hyperfine multiplets. It is found that the resulting charm mass is consistent regardless of the choice of either the ground- or excited-state pairs in the S -wave charmonia.

Both the spin-independent central [$V_C^{2S}(r)$] and spin-spin [$V_S^{2S}(r)$] parts of the interquark potential determined from $\phi_\Gamma^{2S}(r)$ within the time-independent BS amplitude method are basically analogous to those of the $1S$ states, $V_C^{1S}(r)$ and $V_S^{1S}(r)$. The large discrepancies are limited in the particular region, where subtlety is involved in the calculation of $\nabla^2 \phi_\Gamma / \phi_\Gamma$ due to the almost zero value of ϕ_Γ that happens near the node of $\phi_\Gamma^{2S}(r)$ or at long distances with large statistical uncertainties.

To overcome the statistical issues on $\phi_\Gamma^{2S}(r)$, the new time-dependent BS amplitude method was applied only for the analysis of both $V_C^{2S}(r)$ and $V_S^{2S}(r)$. The spin-independent central potential $V_C^{2S}(r)$ is identical to $V_C^{1S}(r)$ within the current statistical precision, while the discrepancy between the spin-spin potentials, $V_S^{1S}(r)$ and $V_S^{2S}(r)$, still remains more or less visible near the node location.

Although we do not rule out the possibility that different sizes of the S - D mixing effect on the J/ψ and $\psi(2S)$ states may lead to some difference in the spin-spin potential, the difference between $V_S^{1S}(r)$ and $V_S^{2S}(r)$ is not statistically significant. Therefore, our results suggest that the possible S - D mixing, which is assumed to be negligible in our current analysis, is not a leading effect for both the J/ψ and $\psi(2S)$ states.

We thus conclude that a universal interquark potential and a unique quark mass can be simultaneously defined in a series of the BS amplitudes from the ground state to excited states. What this means is two-fold: (1) it ensures the reliability of the time-dependent approach in the BS amplitude method for the $Q\bar{Q}$ system, and (2) it strongly supports the validity of the potential description for the charmonium system, at least below the

open-charm threshold.

We plan to extend our research to determine all spin-dependent potentials including the tensor and spin-orbit forces and also intend to take into account the S - D mixing effect on the J/ψ and $\psi(2S)$ states in future analysis.

Acknowledgments

We thank the PACS-CS Collaboration for making their (2+1)-flavor gauge configurations available through ILDG/JLDG. Numerical calculations reported here were partially carried out on the COMA (PACS-IX) system at the CCS, University of Tsukuba, and LX406Re-2 at the Cyberscience Center, Tohoku University.

-
- [1] E. Eichten, K. Gottfried, T. Kinoshita, J. B. Kogut, K. D. Lane and T. M. Yan, The Spectrum of Charmonium, *Phys. Rev. Lett.* **34**, 369 (1975); **36**, 1276(E) (1976).
 - [2] S. Godfrey and N. Isgur, Mesons in a relativized quark model with chromodynamics, *Phys. Rev. D* **32**, 189 (1985).
 - [3] T. Barnes, S. Godfrey, and E. S. Swanson, Higher charmonia, *Phys. Rev. D* **72**, 054026 (2005).
 - [4] G. S. Bali, QCD forces and heavy quark bound states, *Phys. Rep.* **343**, 1 (2001).
 - [5] N. Brambilla, A. Pineda, J. Soto, and A. Vairo, Effective field theories for heavy quarkonium, *Rev. Mod. Phys.* **77**, 1423 (2005).
 - [6] Y. Koma, M. Koma, and H. Wittig, Nonperturbative Determination of the QCD Potential at $O(1/m)$, *Phys. Rev. Lett.* **97**, 122003 (2006).
 - [7] Y. Koma and M. Koma, Spin-dependent potentials from lattice QCD, *Nucl. Phys.* **B769**, 79 (2007).
 - [8] A. Laschka, N. Kaiser, and W. Weise, Charmonium potentials: Matching perturbative and lattice QCD, *Phys. Lett. B* **715**, 190 (2012).
 - [9] N. Ishii, S. Aoki, and T. Hatsuda, The Nuclear Force from Lattice QCD, *Phys. Rev. Lett.* **99**, 022001 (2007).
 - [10] S. Aoki, T. Hatsuda, and N. Ishii, Theoretical foundation of the nuclear force in QCD and its applications to central and tensor forces in quenched lattice QCD simulations, *Prog. Theor. Phys.* **123**, 89 (2010).
 - [11] Y. Ikeda and H. Iida, The antiquark-quark potential from Bethe-Salpeter amplitudes on lattice, *Proc. Sci. LATTICE2010* (2010) 143.
 - [12] Y. Ikeda and H. Iida, Quark-antiquark potentials from Nambu-Bethe-Salpeter amplitudes on lattice, *Prog. Theor. Phys.* **128**, 941 (2012).
 - [13] T. Kawanai and S. Sasaki, Interquark Potential with Finite Quark Mass from Lattice QCD, *Phys. Rev. Lett.* **107**, 091601 (2011).
 - [14] T. Kawanai and S. Sasaki, Charmonium potential from full lattice QCD, *Phys. Rev. D* **85**, 091503 (2012).
 - [15] T. Kawanai and S. Sasaki, Heavy quarkonium potential from Bethe-Salpeter wave function on the lattice, *Phys. Rev. D* **89**, 054507 (2014).
 - [16] T. Kawanai and S. Sasaki, Potential description of charmonium and charmed-strange mesons from lattice QCD, *Phys. Rev. D* **92**, 094503 (2015).
 - [17] C. Michael, Adjoint Sources in Lattice Gauge Theory, *Nucl. Phys.* **B259**, 58 (1985).
 - [18] M. Lüscher and U. Wolff, How to calculate the elastic scattering matrix in two-dimensional quantum field theories by numerical simulation, *Nucl. Phys.* **B339**, 222 (1990).
 - [19] S. Sasaki and T. Yamazaki, Signatures of S-wave bound-state formation in finite volume, *Phys. Rev. D* **74**, 114507 (2006).
 - [20] M. Göckeler, H. A. Kastrup, J. Westphalen, and F. Zimmermann, Scattering phases on finite lattices in the broken phase of the four-dimensional $O(4)$ ϕ^4 theory, *Nucl. Phys.* **B425**, 413 (1994).
 - [21] J. Liang, Y. Chen, W. F. Chiu, L. C. Gui, M. Gong, and Z. Liu, Wave functions of $SU(3)$ pure gauge glueballs on the lattice, *Phys. Rev. D* **91**, 054513 (2015).
 - [22] W. E. Caswell and G. P. Lepage, Reduction of the Bethe-Salpeter equation to an equivalent schrodinger equation, with applications, *Phys. Rev. A* **18**, 810 (1978).
 - [23] N. Ishii, S. Aoki, T. Doi, T. Hatsuda, Y. Ikeda, T. Inoue, K. Murano, H. Nemura, and K. Sasaki (HAL QCD Collaboration), Hadron-hadron interactions from imaginary-time Nambu-Bethe-Salpeter wave function on the lattice, *Phys. Lett. B* **712**, 437 (2012).
 - [24] K. Nochi, T. Kawanai, and S. Sasaki (to be published).
 - [25] S. Aoki *et al.* (PACS-CS Collaboration), 2+1 flavor lattice QCD toward the physical point, *Phys. Rev. D* **79**, 034503 (2009).
 - [26] A. X. El-Khadra, A. S. Kronfeld, and P. B. Mackenzie, Massive fermions in lattice gauge theory, *Phys. Rev. D* **55**, 3933 (1997).
 - [27] S. Aoki, Y. Kuramashi, and S. i. Tominaga, Relativistic heavy quarks on the lattice, *Prog. Theor. Phys.* **109**, 383 (2003).
 - [28] Y. Kayaba, S. Aoki, M. Fukugita, Y. Iwasaki, K. Kanaya, Y. Kuramashi, M. Okawa, A. Ukawa, and T. Yoshié (CP-PACS Collaboration), First nonperturbative test of a relativistic heavy quark action in quenched lattice QCD, *J. High Energy Phys.* 02 (2007) 019.

- [29] Y. Namekawa *et al.* (PACS-CS Collaboration), Charm quark system at the physical point of 2+1 flavor lattice QCD, Phys. Rev. D **84**, 074505 (2011).
- [30] S. Güsken, A study of smearing techniques for hadron correlation functions, Nucl. Phys. Proc. Suppl. **17**, 361 (1990).
- [31] C. Alexandrou, S. Güsken, F. Jegerlehner, K. Schilling, and R. Sommer, The static approximation of heavy-light quark systems: A systematic lattice study, Nucl. Phys. **B414**, 815 (1994).
- [32] F. Berruto, T. Blum, K. Orginos, and A. Soni, Calculation of the neutron electric dipole moment with two dynamical flavors of domain wall fermions, Phys. Rev. D **73**, 054509 (2006).
- [33] D. Mohler and R. M. Woloshyn, D and D_s meson spectroscopy, Phys. Rev. D **84**, 054505 (2011).
- [34] S. Sasaki, Lattice Study of Exotic $S = +1$ Baryon, Phys. Rev. Lett. **93**, 152001 (2004).
- [35] In Ref. [22], for QED bound states such as positronium or muonium, the reduction of the Bethe-Salpeter equation in quantum field theory to an equivalent Schrödinger equation in quantum mechanics was discussed in a systematic perturbation series. The wave functions and the interaction kernel are, however, described in momentum space rather than in coordinate space.
- [36] If it is not the case, the quark kinetic mass obtained from Eq.(10) and the interquark potentials determined from Eqs. (11) and (12) may just have the dependence of the choice of either the ground- or excited-state.
- [37] International Lattice Data Grid/Japan Lattice Data Grid, <http://www.jldg.org>.
- [38] It is reminded that masses of $1P$ -charmonium states (χ_{c0} , χ_{c1} and h_c) in the current set-up are fairly consistent with the experimental values, as studied in Refs. [14, 16].
- [39] The P -wave DD^* and $D^*\bar{D}^*$ threshold energies are determined as 3.973(12) GeV and 4.133(17) GeV with the measured D^* meson mass [$M_{D^*} = 2.022(8)$ GeV] in our calculation. These are much above our results of the $\eta_c(2S)$ and $\psi(2S)$ masses.
- [40] For the S -wave states, we simply use a relation of $\sum_{\mathbf{r}} |\phi_{n,\Gamma}(\mathbf{r})|^2 = 4\pi \int dr |u_{n,\Gamma}(r)|^2$ and then perform one-dimensional numerical integration in r space by both the Simpson 1/3 formula and the trapezoid formula in this study.